Journal of Alloys and Compounds 499 (2010) 80–89

Contents lists available at ScienceDirect

Journal of Alloys and Compounds

journal homepage: www.elsevier.com/locate/jallcom

First-principles study of the ternary semiconductor alloys (Ga,Al)(As,Sb)

F. El Haj Hassan[a,b,*], A. Breidi[a,c], S. Ghemid[d], B. Amrani[d], H. Meradji[d], O. Pagès[c]

[a] Université Libanaise, Faculté des sciences (I), Laboratoire de Physique de Matériaux, Elhadath, Beirut, Lebanon
[b] Condensed Matter Section, The Abdus Salam International Centre for Theoretical Physics (ICTP), Strada Costiera 11, 34014 Trieste, Italy
[c] Laboratoire de Physique des Milieux Denses, Université Paul Verlaine—Metz, 1 Bd. Arago, 57078 Metz, France
[d] Laboratoire LPR, Département de Physique, Faculté des Sciences, Université de Annaba, Mascara 29000, Algeria

ARTICLE INFO

Article history:
Received 27 October 2009
Received in revised form 11 February 2010
Accepted 15 February 2010
Available online 23 February 2010

PACS:
61.66.Dk
71.15.Ap
71.15.Mb
71.20.−b
77.22.Ch

Keywords:
FP-LAPW
DFT
Ternary alloys
Band structures
Dielectric function
Critical temperature

ABSTRACT

First-principles calculations are performed to study the structural, electronic, optical and thermodynamic properties of technologically important $Al_xGa_{1-x}As$, $Al_xGa_{1-x}Sb$, $GaAs_xSb_{1-x}$ and $AlAs_xSb_{1-x}$ ternary alloys using the full potential-linearized augmented plane wave plus local orbitals method within the density functional theory. We use both Wu–Cohen and Engel–Vosko generalized gradient approximations of the exchange-correlation energy that are based on the optimization of total energy and corresponding potential, respectively. Our investigation on the effect of composition on lattice constant, bulk modulus, ionicity, band gap, effective mass and refractive index for ternary alloys shows almost non-linear dependence on the composition. The bowing of the fundamental gap versus composition predicted by our calculations is in good agreement with available experiment data. The different roles of structural and chemical effects on the gap bowing and its variation with composition are identified and discussed. It is found that charge-exchange effect overwhelms the other contributions to the gap bowing. Besides, a regular-solution model is used to investigate the thermodynamic stability of the alloys which mainly indicates a phase miscibility gap. In addition, the quasi-harmonic Debye model is applied to determine the thermal properties at room temperature.

1. Introduction

Semiconductor alloys provide a natural means of tuning the magnitude of the forbidden gap and other material parameters so as to optimize and widen the applications of semiconductor devices [1]. With the advent of small-structure systems, such as quantum wells and superlattices, the effects of alloy compositions, size, device geometry, doping and controlled lattice strain can be combined to achieve maximum tenability [2].

The III–V semiconductor alloys are promising candidates for many device applications such as high-speed electronic and long wavelength photonic devices because their band gaps cover a wide spectral range [3,4]. Among these materials, the (Al,Ga)(As,Sb) ternary alloys are covering wavelengths between the visible and infrared region. $Al_xGa_{1-x}As$ is the most important and the most studied III–V semiconductor alloy, its key role in a variety of transistor and optoelectronic devices has necessitated a precise knowledge of the fundamental energy gap as well as the alignment of the three main conduction-band valleys [5–9]. $Al_xGa_{1-x}Sb$ is an important material employed in high-speed electronic covering the 1.30–1.55 μm range which is required for infrared optical fiber communication system [10–13]. $GaAs_xSb_{1-x}$ is very attractive material for optoelectronic applications. They are widely used as a material for the active region of light-emitting diodes and photo detectors for the wave lengths 1.3–1.6 mm [14–16]. $AlAs_xSb_{1-x}$ is a versatile large-gap barrier material that can be lattice matched to InP, InAs, or GaSb substrates [8,17–19]. The studied ternary alloys (Ga,Al)(As,Sb) form a border of the $Al_xGa_{1-x}As_ySb_{1-y}$ quaternary alloys which are interesting materials in the commercial technologies [20].

In spite of the importance of ternary alloys for device applications, limited theoretical work on the $Al_xGa_{1-x}As$, $Al_xGa_{1-x}Sb$, $GaAs_xSb_{1-x}$ and $AlAs_xSb_{1-x}$ ternary alloys has been carried out because of computational complexities and difficulties associate with disorder in the alloys, hence in order to complete the exciting experimental and theoretical works and to provide a basis for understanding future device concepts and applications, we have

* Corresponding author at: Université Libanaise, Faculté des sciences (I), Laboratoire de Physique de Matériaux, Elhadath, Beirut, Lebanon. Tel.: +961 5 460494; fax: +961 5 461496.
E-mail address: hassan.f@ul.edu.lb (F. El Haj Hassan).

0925-8388/$ – see front matter © 2010 Elsevier B.V. All rights reserved.
doi:10.1016/j.jallcom.2010.02.121

Table 1
Calculated lattice parameter a, bulk modulus B, and gap energy E_g for the binary compounds in zinc-blende structure at equilibrium volume. Experimental data are also shown for comparison. (Ours: this work; WC: Wu and Cohen GGA; PBE: Perdew–Burke–Ernzerhof GGA; EV: Engel–Vosko GGA).

	a (Å)			B (GPa)			E_g (eV)		
	Our work		exp.	Our work		Exp.	Our work		Exp.
	WC	PBE		WC	PBE		WC	EV	
GaAs	5.666	5.754	5.653[a]	69.6	60.9	75.5[a]	0.336	0.966	1.424 (E_g^{Γ})[a]
GaSb	6.115	6.221	6.096[a]	51.9	45.9	56.3[a]	0.000	0.396	0.726 (E_g^{Γ})[a]
AlAs	5.678	5.736	5.661[a]	72.3	66.8	78.1[a]	1.861	2.104	2.170 (E_g^{X})[a]
AlSb	6.160	6.232	6.135[b]	54.9	49.7	55.1[c]	1.343	1.470	1.696 (E_g^{X})[b]

[a] Ref. [9].
[b] Ref. [8].
[c] Ref. [31].

employed density functional theory (DFT) to some properties of these ternary alloys.

The present work aims to extend the study of the composition dependence of the energy band gap and to investigate in detail the physical origin of the band gap bowing b. The refractive indices and the optical dielectric constants of the materials have been investigated as a function of composition. In addition to the consideration of the electronic and structural properties, we have studied the phase stability. Finally, the quasi-harmonic Debye model was successfully applied to determine the thermal properties. In the subsequent text, the computational details are given in Section 2. The results are presented and discussed in Section 3. Section 4 is the conclusion.

2. Computational details

Describing random alloys by periodic structures will clearly introduce spurious correlations beyond certain distance. Preventing this problem needs a very large supercell for which first-principle self-consistent calculations are still impractical. However, many physical properties of solids are characterized by microscopic length scales and local randomness of alloys and modifying the large scale randomness of alloys does not affect them. Zunger et al. [21] implemented this fact to construct *Special Quasirandom Structures* (SQS) approach by close reproduction of the perfectly random network for the first few shells around a given site, deferring periodicity errors to more distant neighbors. They argued that this approach, adopted in our calculation, effectively reduces the size of the supercell for studding many properties of random alloys.

We have employed the scalar-relativistic FP-LAPW+lo method [22–24] within the framework of DFT [25] as implemented in WIEN2K [26] code. For structural properties the exchange-correlation potential was calculated using the generalized gradient approximation (GGA) in the new form (WC) proposed by Wu and Cohen [27] which is a improved form of the most popular Perdew–Burke–Ernzerhof (PBE) GGA [28]. In addition, and for electronic properties only, we also applied the Engel–Vosko (EV) scheme [29]. In the FP-LAPW+lo method, the wave function, charge density and potential were expanded by spherical harmonic functions inside non-overlapping spheres surrounding the atomic sites (muffin-tin spheres) and by plane waves basis set in the remaining space of the unit cell (interstitial region). A mesh of 35 special k-point for binary compounds and 27 special k-point for ternary alloys were taken in the irreducible edge of Brillouin zone. The maximum l quantum number for the wave function expansion inside atomic spheres was confined to $l_{max} = 10$. The plane wave cutoff of $K_{max} = 8.0/R_{MT}$ (R_{MT} is the smallest muffin-tin radius in the unit cell) is chosen for the expansion of the wave functions in the interstitial region while the charge density is Fourier expanded up to $G_{MAX} = 14(Ryd)^{1/2}$. The muffin-tin radius was assumed to be 2.0, 2.1, 2.2 and 2.3 a.u. for Al, Ga, As and Sb atoms, respectively. Both the plane wave cutoff and the number of k-point were varied to ensure total energy convergence. Our calculations for valence electrons were performed in a scalar-relativistic approximation, with neglecting spin–orbit coupling, while the core electrons were treated fully relativistic.

3. Results and discussion

Before handling the main steps of the present work, let us start with a preliminary study of the structural and electronic properties of the zinc-blend binary compounds GaSb, GaAs, AlSb, and AlAs. The calculated total energies using GGA scheme at many different volumes around equilibrium were fitted by the Murnaghon's equation-of-state [30]. The equilibrium lattice parameter, bulk modulus and gap energy were presented and compared with the experimental data in Table 1. It is clearly seen that the WC calculated lattice constants and bulk modulus are more accurate than those of PBE. A small difference (less than 1%) could be observed between WC calculated and experimental lattice constants which can be attributed to the general trend that GGA usually overestimates this parameters [32,33].

The computed band structures of binary compounds using WC and EV schemes indicate a direct band gap for GaAs and GaSb, while AlAs and AlSb are an indirect band gap with the X–L–Γ ordering of the conduction valley minima. In fact, GGA usually underestimates the experimental energy band gap [34,35], this is an intrinsic feature of DFT which is not suitable for describing excited-state properties. However, it is widely accepted that GGA electronic band structures are qualitatively in good agreement with experiments as regards the ordering of the energy levels and the shape of the bands. Engel and Vosko by considering this shortcoming of the energy gap constructed a new functional form of the GGA which is able to better reproduce exchange potential at the expense of less agreement in exchange energy. This approach (EV) yields a better band splitting. However, in this method, the quantities that depend on an accurate description of exchange energy E_x such as equilibrium volumes and bulk modulus are in poor agreement with experiment. Therefore, in order to obtain more accurate energy band gaps in our calculations, we applied EV to the theoretical lattice constants obtained by WC throughout this paper.

3.1. Structural properties

The second step of our calculations was to study the structural properties of $Al_xGa_{1-x}As$, $Al_xGa_{1-x}Sb$, $GaAs_xSb_{1-x}$ and $AlAs_xSb_{1-x}$ alloys. The lattice structures have been modeled at some selected compositions $x = 0.25$, 0.5, 0.75. For the considered structures, we perform the structural optimization by minimizing the total energy with respect to the cell parameters and also the atomic positions (as prototype, Table 2 summarizes the atomic positions of

Table 2
Atomic positions for $GaAs_xSb_{1-x}$ alloys.

x	Atom	Atomic positions
0.25 Luzonite	Ga	(1/4 1/4 1/4), (3/4 3/4 1/4), (3/4 1/4 3/4), (1/4 3/4 3/4)
	As	(0 0 0)
	Sb	(0 1/2 1/2), (1/2 0 1/2), (1/2 1/2 0)
0.5 Chalcopyrite	Ga	(0 0 0), (0 1/2 2/8), (1/2 /1/2 4/8), (1/2 0 6/8)
	As	(1/4 1/4 1/8), (3/4 3/4 1/8), (3/4 1/4 3/8), (1/4 3/4 3/8), (1/4 1/4 5/8), (3/4 3/4 5/8), (3/4 1/4 7/8), (1/4 3/4 7/8)
	Sb	(1/2 1/2 0), (1/2 0 2/8), (0 0 4/8), (0 1/2 6/8)
0.75 Luzonite	Ga	(1/4 1/4 1/4), (3/4 3/4 1/4), (3/4 1/4 3/4), (1/4 3/4 3/4)
	As	(0 1/2 1/2), (1/2 0 1/2), (1/2 1/2 0)
	Sb	(0 0 0)

$GaAs_xSb_{1-x}$). For the compositions $x = 0.25$ and 0.75 the simplest structure is an eight-atom simple cubic cell (luzonite): the anions with the lower concentration form a regular simple cubic lattice. For the composition $x = 0.5$, the smallest ordered structure is a four-atom tetragonal cell, corresponding to the (0 0 1) superlattice. This structure is strongly anisotropic, and thus not very suitable for simulating random alloys which are macroscopically isotropic. We consider therefore the chalcopyrite structure, which has a 16-atom tetragonal cell. Our calculated lattice constants at different composition of $Al_xGa_{1-x}As$, $Al_xGa_{1-x}Sb$, $GaAs_xSb_{1-x}$ and $AlAs_xSb_{1-x}$ alloys, as shown in Fig. 1, were found to vary almost linearly following the Vegard's law [36] with a marginal upward bowing parameters equal to −0.008 (Exp. [6]: +0.007 Å), −0.016, −0.098 and −0.099 Å, respectively. However, violation of Vegard's law has been reported in semiconductor alloys both experimentally [37,38] and theoretically [39].

A deviation of the bulk modulus from the linear concentration dependence (see Fig. 1) with downward bowing equal to 0.2 (Exp. [6]: 0.26 GPa), 1.9, 8.4 (Exp. [6]: 19 GPa) and 10.1 GPa for $Al_xGa_{1-x}As$, $Al_xGa_{1-x}Sb$, $GaAs_xSb_{1-x}$ and $AlAs_xSb_{1-x}$ alloys, respectively was observed. It should be noted that the values of the bulk modulus bowing are small for the two first alloys which should be mainly due to the small mismatches of the bulk modulus of the constitute binary compounds. A more precise comparison for the behavior of the $GaAs_xSb_{1-x}$ and $AlAs_xSb_{1-x}$ ternary alloys (Fig. 1) shows that a decrease of the lattice constant is accompanied by a decrease of the bulk modulus while for the other two ternary alloys a reverse phenomenon was observed. It represents bond strengthening or weakening effects induced by changing the composition.

The charge density is an appropriate tool that provides us a better understanding of the bonding character in these compounds and FP-LAPW gives an accurate description of the valence charge density. Ionic charge obviously plays a decisive role in the physics of alloys and they are yet quantities difficult to assess in a consistent and meaningful way. Even if we know the distribution of the valence charge in a semiconductor, the ionic charges are arbitrary, depending on the way we divide the space assigned to the individual atoms. One can correlate the valence charge density to the ionicity factor through an empirical formula [40], which has been successfully applied to other A^NB^{8-N} compounds [41]. The calculated ionicity values for GaSb, GaAs, AlSb and AlAs compounds are respectively, 0.211 (0.261), 0.275 (0.310), 0.191 (0.250) and 0.225 (0.274). Our WC calculated values agree well with the corresponding Phillips results [42] presented inside the parentheses. The ionicity decreases when the group VI anion changes from As to Sb. In Fig. 2, we show the ionicity of the bonds at different concentrations which decreases as the lattice constant increases and vice versa. It is relevant to note that for all the four alloys the ionicity changes almost linearly by going from $x = 0$ to $x = 1$ with slopes equal to −0.998, −0.997, 0.998 and 0.997 for $Al_xGa_{1-x}As$, $Al_xGa_{1-x}Sb$, $GaAs_xSb_{1-x}$ and $AlAs_xSb_{1-x}$ alloys, respectively.

3.2. Electronic prosperities

The crucial role of the four studied ternary alloys in a variety of technologically devices has necessitated precise knowledge of the fundamental energy gap as well as the alignment of the three main conduction-band valleys. Investigations are complicated by the fact that whereas GaSb and GaAs are a direct-gap material with Γ–L–X valley ordering, AlSb and AlAs are an indirect-gap material with exactly the reverse ordering. Particular attention has been devoted to the crossover point, at which the Γ and X valley minima have the same energies. The EV calculated band gap energy is displayed

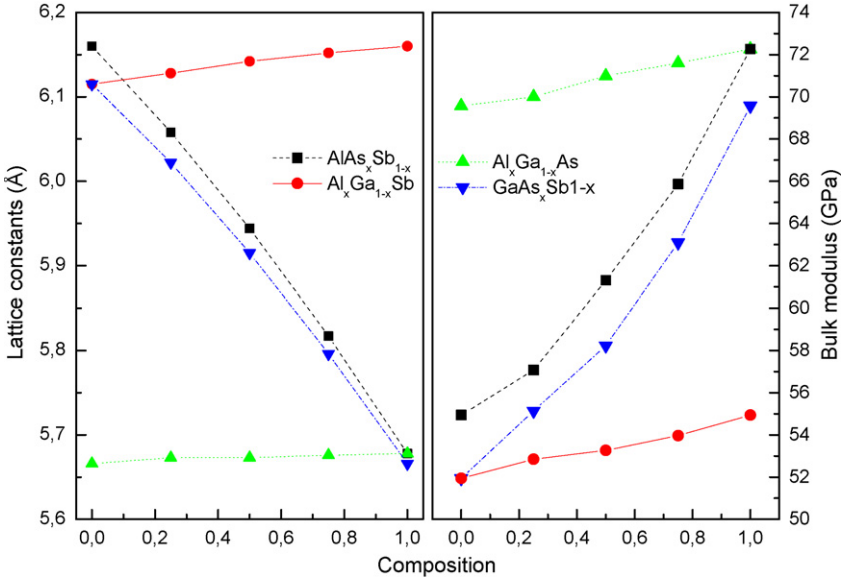

Fig. 1. Composition dependence of the calculated lattice constant (left panel) and bulk modulus (right panel) of the ternary alloys of interest using WC-GGA.

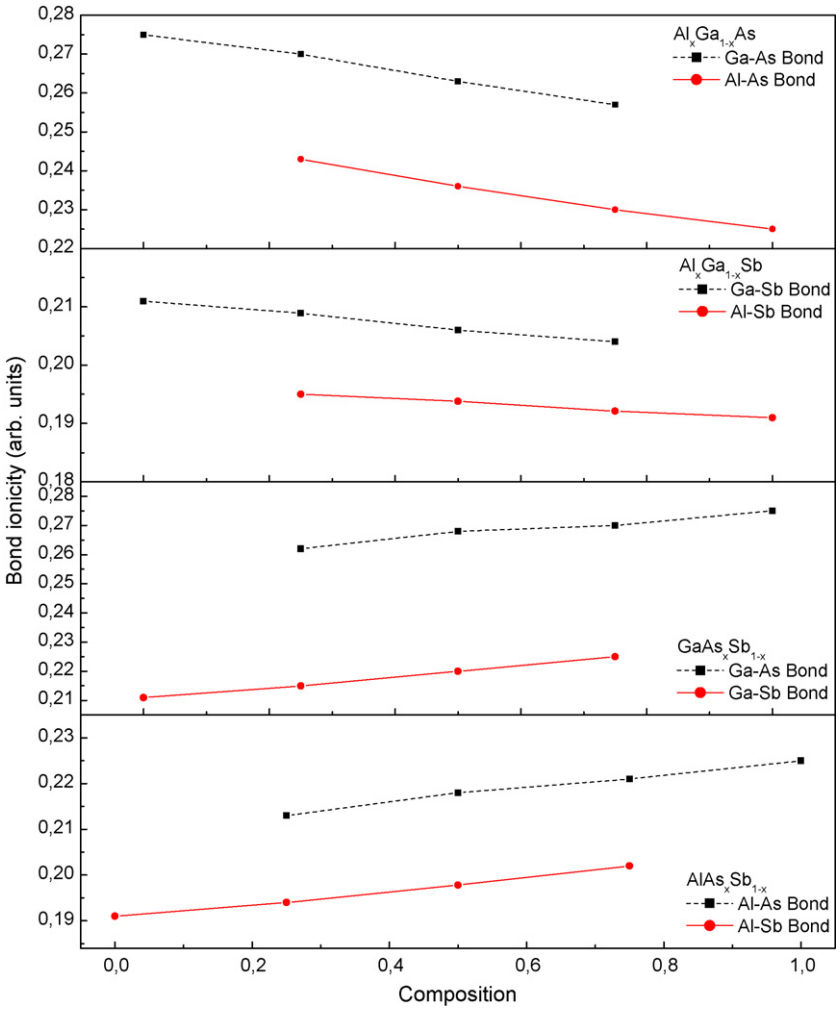

Fig. 2. The ionicity variation of the calculated bonds versus concentration.

in Fig. 3. The crossover of direct–indirect-gap occurs at x equals to 0.43 (Exp. [6]: 0.45) and 0.25 (Exp. [8]: 0.27) for $Al_xGa_{1-x}As$ and $Al_xGa_{1-x}Sb$ alloys, respectively.

However one may note that due to the systematic underestimation of the energy band gap in local density approximation (LDA) (GGA)-DFT studies, our results are not accurate enough to be applicable in industry. This obstacle can be overcome by taking into account the scissor correction scheme [43], which in its simplest form requires a rigid shift of the unoccupied part of the DFT-GGA band structure. To do this correction, one may use the experimental values of binary compounds band gaps in Eq. (1) along with the EV calculated band gap bowing parameters. We have done this scissor type correction for all ternary alloys and the results are presented in Fig. 3 (lines without symbols).

The band gap increases non-linearly with increasing of the concentration x providing a positive gap bowing. Indeed it is a general trend to describe the band gap of an alloy AB_xC_{1-x} in terms of the pure compound energy gap E_{AB} and E_{AC} by the semi-empirical formula:

$$E_g = xE_{AB} + (1-x)E_{AC} - x(1-x)b, \tag{1}$$

where the curvature b is commonly known as gap bowing parameter. The results, obtained by quadratic fit, are presented in Table 3.

In order to better understand the physical origins of the gap bowing parameter b, Bernard and Zunger [45] decompose it into three contributions resulting from volume deformation, charge-exchange, and structural relaxation. The overall gap bowing coefficient at $x = 0.5$ measures the change in band gap according to the reaction:

$$AB(a_{AB}) + AC(a_{AC}) \rightarrow AB_{0.5}C_{0.5}(a_{eq}), \tag{2}$$

where a_{AB} and a_{AC} are the equilibrium lattice constants of the binary compounds AB and AC, respectively; and a_{eq} is the alloy equilibrium lattice constant.

First, volume deformation (b_{VD}) represents changes in the band gaps of the bulk materials that are compressed and dilated, respectively, from their equilibrium lattice constants to the intermediate alloy one $a = a(x)$, according to the following reaction:

$$AB(a_{AB}) + AC(a_{AC}) \xrightarrow{VD} AB(a) + AC(a), \tag{3}$$

So that

$$b_{VD} = 2[\varepsilon_{AB}(a_{AB}) - \varepsilon_{AB}(a) + \varepsilon_{AC}(a_{AC}) - \varepsilon_{AC}(a)]. \tag{4}$$

Secondly, charge-exchange b_{CE} represents the change in the band gap upon bringing together the constituents, already prepared at the lattice constant a, without permitting any sublattice relaxation. The formal reaction is

$$AB(a) + AC(a) \xrightarrow{CE} AB_{0.5}C_{0.5}(a). \tag{5}$$

This term includes charge-transfer effects due to the different bonding behaviors of the two constituents; the contribution of this

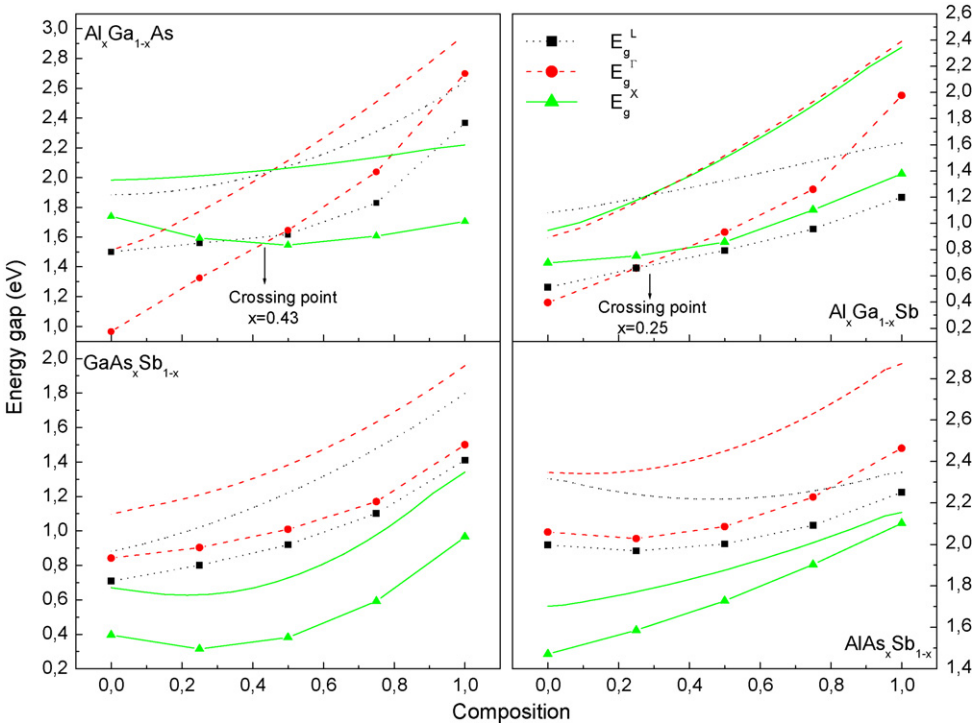

Fig. 3. Energy band gap as a function of composition for the ternary alloys. Lines symbols: calculated values using EV, lines: scissor corrected values. The top axis is exactly the same as the bottom axis.

charge transfer to the bowing is hence:

$$b_{CE} = 2[\varepsilon_{AB}(a) + \varepsilon_{AC}(a) - 2\varepsilon_{ABC}(a)]. \quad (6)$$

The final step measures changes due to the structural relaxation in passing from the unrelaxed to the relaxed alloy by b_{SR},

$$AB_{0.5}C_{0.5}(a) \xrightarrow{SR} AB_{0.5}C_{0.5}(a_{eq}), \quad (7)$$

$$b_{SR} = 4[\varepsilon_{ABC}(a) - \varepsilon_{ABC}(a_{eq})]. \quad (8)$$

The addition of the three contributions (4), (6), and (8) leads to the total bowing parameter b. The computed bowing coefficients b together with the three different contributions for alloys of interest is given in Table 3. The calculated quadratic parameters (gap bowing) are very close to their corresponding results obtained by Zunger approach. The smallest contribution of volume deformation term b_{VD} is attributed to the marginal mismatch of the lattice constant occurring between the bulk materials as shown in the previous section. The total gap bowing for all the four alloys were found

Table 3
Decomposition of the optical bowing into volume deformation (VD), charge-exchange (CE), and structural relaxation (SR) contributions compared with that obtained by a quadratic fit and other predictions (all values are in eV).

	Our work						Exp.[a]		
	Zunger approach			Quadratic fits					
	L	Γ	X	L	Γ	X	L	Γ	X
Al$_x$Ga$_{1-x}$As									
b_{VD}	0.001	0.014	0.001						
b_{CE}	1.536	0.515	0.163						
b_{SR}	0.287	−0.042	−0.005						
b	1.824	0.487	0.168	1.888	0.455	0.209	1.705	0.438	0.16
Al$_x$Ga$_{1-x}$Sb									
b_{VD}	0.006	−0.001	0.001						
b_{CE}	0.586	0.409	0.082						
b_{SR}	0.009	0.046	0.009						
b	0.601	0.454	0.092	0.720	0.530	0.202	0.64	0.47	0.05
GaAs$_x$Sb$_{1-x}$									
b_{VD}	0.017	0.085	0.010						
b_{CE}	0.222	0.443	0.324						
b_{SR}	0.014	0.669	0.012						
b	0.253	1.197	0.454	0.362	1.371	0.481	0.248	1.2	0.31
AlAs$_x$Sb$_{1-x}$									
b_{VD}	0.059	0.002	0.012						
b_{CE}	0.405	0.722	0.222						
b_{SR}	0.032	−0.025	−0.007						
b	0.496	0.699	0.227	0.489	0.724	0.322	0.474	0.691	0.25

[a] Ref. [44].

to be mainly caused by the charge-exchange b_{CE}, this is related to the electronegativity [46] Mismatch for Al (1.6), Ga (1.81), As (2.18) and Sb (2.05). The contribution of the structural relaxation term b_{SR} to the bowing parameter, although smaller than b_{CE}, is not ignorable (b_{SR} sometimes negative).

It is also interesting to discuss at the end of the band structure study, the effective masses of electrons (m_e^*) and holes (m_h^*), which are important for the excitonic compounds. We have calculated the effective masses using EV scheme. A theoretical effective mass in general turns out to be a tensor with nine components. However, for a very idealized simple case where $E(k)$ is a parabola at $k = 0$ (high symmetry point Γ), the effective mass becomes a scalar. We have computed the effective masses of electrons and holes both at the conduction-band minima and valance-band maxima. The results obey the following variations:

$$Al_xGa_{1-x}As \Rightarrow \begin{cases} m_e^*(x) = 0.056 - 0.179\,x + 0.325\,x^2 \\ m_h^*(x) = 0.242 + 0.174\,x - 0.066\,x^2 \end{cases}, \quad (9)$$

$$Al_xGa_{1-x}Sb \Rightarrow \begin{cases} m_e^*(x) = 0.073 - 0.21\,x + 0.482\,x^2 \\ m_h^*(x) = 0.337 + 0.101\,x - 0.001\,x^2 \end{cases}, \quad (10)$$

$$GaAs_xSb_{1-x} \Rightarrow \begin{cases} m_e^*(x) = 0.057 + 0.034\,x + 0.018\,x^2 \\ m_h^*(x) = 0.338 + 0.078\,x + 0.014\,x^2 \end{cases}, \quad (11)$$

$$AlAs_xSb_{1-x} \Rightarrow \begin{cases} m_e^*(x) = 0.187 - 0.344\,x + 0.395\,x^2 \\ m_h^*(x) = 0.250 + 0.079\,x + 0.016\,x^2 \end{cases}. \quad (12)$$

Accordingly, the electron effective masses increase non-linearly with increasing of concentration x, while the hole effective masses variation is almost linear.

3.3. Optical properties

Since the alloys of interest have cubic symmetry, we need to calculate only one dielectric tenor component to completely characterize the linear optical properties. In the following $\varepsilon(\omega)$ is the frequency-dependent dielectric function. The imaginary part $\varepsilon_2(\omega)$ of the frequency-dependent dielectric function is given by [47]:

$$\varepsilon_2(\omega) = \frac{e^2\hbar}{\pi m^2\omega^2}\sum_{v,c}\int_{BZ}|M_{cv}(k)|^2\delta[\omega_{cv}(k) - \omega]d^3k. \quad (13)$$

The integral is over the first Brillouin zone, the momentum dipole elements, $M_{cv}(k) = \langle u_{ck}|e.\nabla|u_{vk}\rangle$ where e is the potential vector defining the electric field, are matrix elements for direct transitions between valence-band $u_{vk}(k)$ and conduction-band $u_{ck}(k)$ states, and the energy $\hbar\omega_{cv}(k) = E_{ck} - E_{vk}$ is the corresponding transition energy.

The real part $\varepsilon_1(\omega)$ of the frequency-dependent dielectric function can be derived from the imaginary part using the Kramers–Kronig relations,

$$\varepsilon_1(\omega) = 1 + \frac{2}{\pi}P\int_0^\infty \frac{\omega'\varepsilon_2(\omega')}{\omega'^2 - \omega^2}d\omega', \quad (14)$$

where P implies the principal value of the integral. Knowledge of both real and imaginary parts of the frequency-dependent dielectric function allows the calculation of important optical functions such as the refractive index $n(\omega)$:

$$n(\omega) = \left[\frac{\varepsilon_1(\omega)}{2} + \frac{\sqrt{\varepsilon_1^2(\omega) + \varepsilon_2^2(\omega)}}{2}\right]^{1/2} \quad (15)$$

At low frequency ($\omega = 0$):

$$n(0) = \varepsilon^{1/2}(0) \quad (16)$$

The refractive index and optical dielectric constants are very important to determine the optical and electric properties of the crystal. Advanced applications of these alloys can significantly benefit from accurate index data. The use of fast non-destructive optical techniques for epitaxial layer characterization (determination of thickness or alloy composition) is limited by the accuracy with which refractive indices can be related to alloy composition. These applications require an analytical expression or known accuracy to relate the wavelength dependence of refractive index to alloy composition, as determined from simple techniques as photoluminescence.

In the calculations of the optical properties, a dense mesh of uniformly distributed k-point is required. Hence, the Brillouin zone integration was performed with 816 and 729 k-point in the irreducible part of the Brillouin zone for binary and ternary compounds, respectively. Broadening is taken to be 0.2 eV. The EV scheme within scissor correction was used in order to perform accurate optical parameter calculations.

Fig. 4 displays the $\varepsilon_2(\omega)$ for our studied alloys, at special composition $x = 0.5$ as prototype, for a radiation up to 12 eV. As can be seen, the linear optical absorption varies from one compound to another. This is attributed to the fact that the conduction bands are different, and the symmetry of the wave functions dictate that the selection rules are fully reflected in the matrix moment elements. Our analysis of the $\varepsilon_2(\omega)$ curves show that the threshold energy (first critical Points) of the dielectric function occurs at about 1.71, 1.01, 0.9 and 1.85 eV for $Al_{0.5}Ga_{0.5}As$, $Al_{0.5}Ga_{0.5}Sb$, $GaAs_{0.5}Sb_{0.5}$ and $AlAs_{0.5}Sb_{0.5}$ alloys, respectively. These points are Γ_v–X_c splitting for $Al_{0.5}Ga_{0.5}As$, $Al_{0.5}Ga_{0.5}Sb$ and AlAs0.5Sb0.5 alloys (Γ_v–Γ_c splitting for $GaAs_{0.5}Sb_{0.5}$ alloy). This gives the threshold for indirect (direct) optical transitions between the highest valence-band and the lowest conduction band. This is known as the fundamental absorption edge. These critical points are followed by small peaks. The main peaks in the spectra are situated at 4.62, 3.83, 4.21 and 4.26 eV for $Al_{0.5}Ga_{0.5}As$, $Al_{0.5}Ga_{0.5}Sb$, $GaAs_{0.5}Sb_{0.5}$ and $AlAs_{0.5}Sb_{0.5}$ alloys, respectively.

According to the Kramers–Kronig dispersion relation, the real part $\varepsilon_1(\omega)$ of the frequency-dependent dielectric function $\varepsilon(\omega)$ is also obtained and displayed in Fig. 4. We note that there are two main peaks in these spectra. Thereafter, $\varepsilon_1(\omega)$ goes to be negative at about 5.10, 5.21, 4.42, and 4.45 eV for $Al_{0.5}Ga_{0.5}As$, $Al_{0.5}Ga_{0.5}Sb$, $GaAs_{0.5}Sb_{0.5}$ and $AlAs_{0.5}Sb_{0.5}$ alloys, respectively.

In Fig. 5 the refractive index at low frequency are plotted. Whereas refractive index bowings of $Al_xGa_{1-x}As$ [−0.045 (Exp. [6]: 0.09)] and $GaAs_xSb_{1-x}$ [−0.028] were found to be small, a deviation from the linear concentration dependence, with values equal to 0.162 and 0.194 for $Al_xGa_{1-x}Sb$ and $AlAs_xSb_{1-x}$ alloys respectively, was observed.

3.4. Thermodynamic properties

We investigate in this part the phase stability of ternary alloys (Ga,Al)(As,Sb) solid solution systems based on the regular-solution model [48]. The Gibbs free energy of mixing for the alloys is expressed as

$$\Delta G_m = \Delta H_m - T\Delta S_m, \quad (17)$$

where

$$\Delta H_m = \Omega x(1 - x), \quad (18)$$

$$\Delta S_m = -R[x\ln x + (1 - x)\ln(1 - x)]. \quad (19)$$

ΔH_m and ΔS_m are the enthalpy and entropy of mixing, respectively, Ω is the interaction parameter which depends on the material, R is the gas constant, and T is the absolute temperature. The mixing enthalpy of alloys can be obtained as the difference in energy

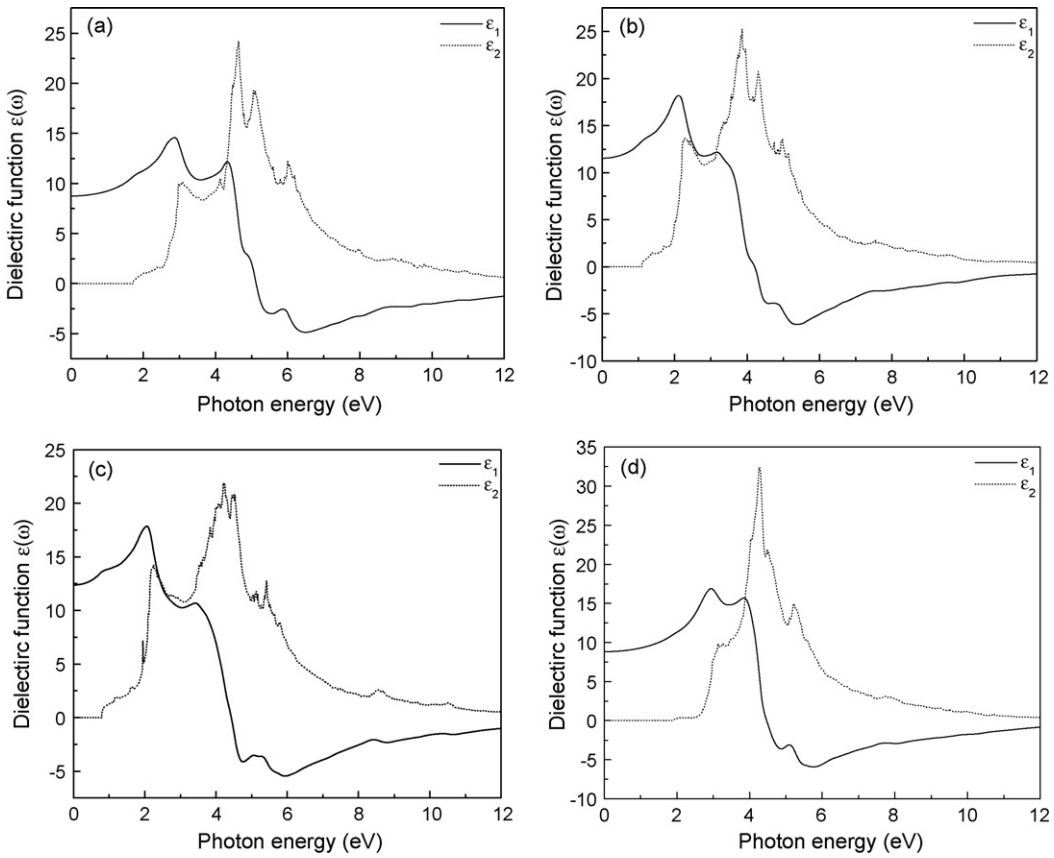

Fig. 4. Calculated real (solid line) and imaginary (dotted lines) parts of the dielectric function of (a) $Al_{0.5}Ga_{0.5}As$, (b) $Al_{0.5}Ga_{0.5}Sb$, (c) $GaAs_{0.5}Sb_{0.5}$ and (d) $AlAs_{0.5}Sb_{0.5}$ ternary alloys.

between the alloy and the weighted sum of the constituents:

$$\Delta H_m = E_{AB_xC_{1-x}} - xE_{AB} - (1-x)E_{AC}. \quad (20)$$

The resulting averaged formation enthalpies of alloys are indicated by the solid circles in Fig. 6. ΔH_m has a maximum near $x = 0.5$. By rewriting expression (18) as $\Omega = \Delta H_m/x(1-x)$ we can calculate, for each x, a value of Ω from the above DFT values of ΔH_m. The only shortcoming we may notice for the regular-solution model for a statistical description of entropy is that the model could be affected by the number of DFT enthalpy values extracted from DFT calculation and, consequently, by the nature of the fit needed. The interaction parameter Ω depending on x is then obtained from a linear fit to the Ω values. The best fit gives:

$$Al_xGa_{1-x}As \Rightarrow 2.317 - 0.253x \text{ (kcal/mole)}, \quad (21)$$

$$Al_xGa_{1-x}Sb \Rightarrow 3.718 + 1.037x \text{ (kcal/mole)}, \quad (22)$$

$$GaAs_xSb_{1-x} \Rightarrow 4.107 + 2.375x \text{ (kcal/mole)}, \quad (23)$$

$$AlAs_xSb_{1-x} \Rightarrow 5.309 + 2.496x \text{ (kcal/mole)}. \quad (24)$$

The average values of the x-dependent Ω in the range $0 \le x \le 1$ obtained from these equations are 6.557, 4.236, 5.294 and 2.190 kcal/mole for $Al_xGa_{1-x}As$, $Al_xGa_{1-x}Sb$, $GaAs_xSb_{1-x}$ and $AlAs_xSb_{1-x}$ alloys, respectively. Next we calculate ΔH_m expressed by Eq. (18) with Eqs. (21)–(24), as drown by the solid curve in Fig. 6. The DFT results of ΔH_m (solid circles) are accurately reproduced by the above ΔH_m curve. Besides, Ω averaged values independent of x is also used to draw ΔH_m, as shown by the dotted curve in Fig. 6. The latter is symmetric around $x = 0.5$, while the x-dependent parameter is asymmetric leading to a slight deviation toward left or right. The effect of this asymmetry will be pronounced in the phase diagram shown later. The formation energies are all positive, this implies that the system has strong tendency to segregate in its constituents at low temperature. At high T, disordered configurations are expected to become favored because of the important increase of the entropic term. Our aim here is to determine the behavior of the alloy between such limits.

Now, we first calculate ΔG_m by using Eqs. (17)–(19). Then we use the Gibbs free energy at different concentrations to calculate the T–x phase diagram which shows the stable, metastable, and unstable mixing regions of the alloy. At a temperature lower than

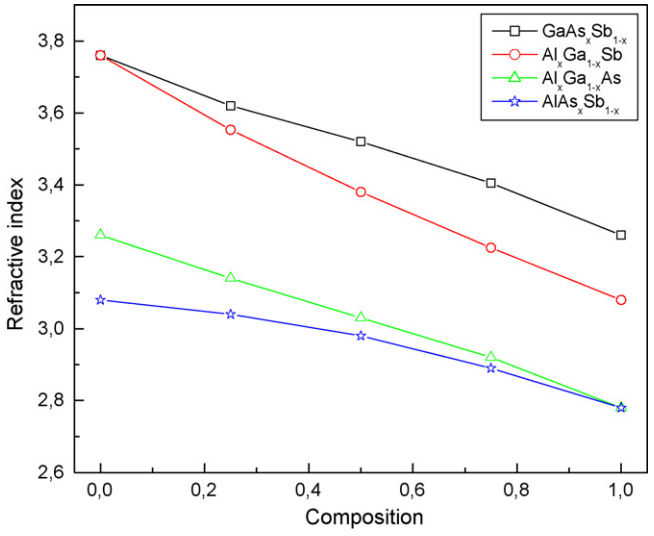

Fig. 5. Calculated refractive index as function of concentration x for the ternary alloys of interest.

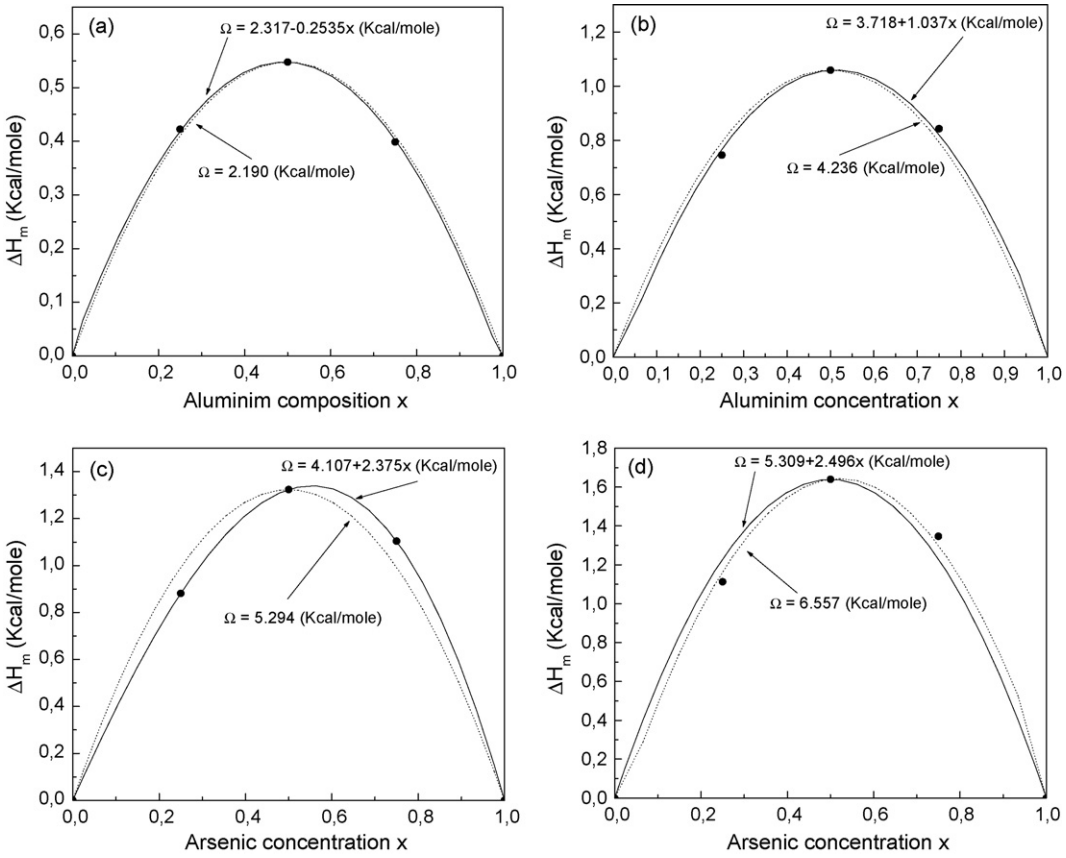

Fig. 6. Enthalpy of mixing ΔH_m as function of concentration for (a) $Al_xGa_{1-x}As$, (b) $Al_xGa_{1-x}Sb$, (c) $GaAs_xSb_{1-x}$ and (d) $AlAs_xSb_{1-x}$ ternary alloys. Solid curve: x-dependent interaction parameters Ω, dotted curve: x-independent interaction parameters Ω.

the critical temperature T_c, the two binodal points are determined as those points at which the common tangent line touches the ΔG_m curves. The two spinodal points are determined as those points at which the second derivative of ΔG_m is zero; $\partial^2(\Delta G_m)/\partial x^2 = 0$.

The composition region between two binodal points is the miscibility gap. Thermodynamically unstable phases may exist metastably in cases where the decomposition kinetics is slow, combined with rapid quenching. Within the miscibility gap, there also exists two inflection spinodal points.

Using the x-dependent interaction parameter Ω, we quantitatively determine the critical temperature T_C and the stable and/or metastable boundary lines. In Fig. 7, we show the resulting phase diagram for alloys of interest. The critical alloy formation temperature occurs at a point where both the first and second derivatives of the free energy are zero, i.e., the plot has no curvature. The miscibility gap disappears at T_C. We observed a critical temperature T_C (at critical composition x_C) of 553 (0.46), 1078 (0.58), 1379 (0.64), and 1693 (0.63) K for $Al_xGa_{1-x}As$, $Al_xGa_{1-x}Sb$, $GaAs_xSb_{1-x}$ and $AlAs_xSb_{1-x}$ alloys, respectively. For our phase diagram, more stable semiconductor alloys are likely to form at high temperature, these results indicate that the alloys is unstable over a wide range of intermediate compositions at normal growth temperature. This purpose can be supported by the work of Guisbiers et al. [5].

Finally, to investigate same thermal properties, we used the quasi-harmonic Debye model [49] in which the non-equilibrium Gibbs function $G^*(V; P, T)$ is written in the form:

$$G^*(V; P, T) = E(V) + PV + A_{vib}[\theta(V); T], \tag{25}$$

where $E(V)$ is the total energy per unit cell, PV corresponds to the constant hydrostatic pressure condition, $\theta(V)$ is the Debye temperature and A_{vib} is the vibrational term which can be written using the Debye model of the phonon density of states as:

$$A_{vib}(\theta; T) = nkT\left[\frac{9\theta}{8T} + 3\ln(1 - e^{-\theta/T}) - D\left(\frac{\theta}{T}\right)\right], \tag{26}$$

where n is the number of atoms per formula unit, $D(\theta/T)$ represents the Debye integral and for an isotropic solid, θ is expressed as:

$$\theta_D = \frac{\hbar}{k}\left[6\pi^2 V^{1/2} n\right]^{1/3} f(\sigma)\sqrt{\frac{B_S}{M}}. \tag{27}$$

M being the molecular mass per unit cell, B_S is the adiabatic bulk modulus, which is approximated given by the static compressibility:

$$B_S \cong B(V) = V\frac{d^2E(V)}{dV^2}. \tag{28}$$

Details on $f(\sigma)$ can be found elsewhere [50,51]. Therefore, the non-equilibrium Gibbs function $G^*(V; P, T)$ as a function of V, P and T can be minimized with respect to volume V:

$$\left[\frac{\partial G^*(V; P, T)}{\partial V}\right]_{P,T} = 0. \tag{29}$$

By solving Eq. (29), one can obtain the thermal equation-of-state (EOS) $V(P, T)$. The heat capacity C_V and the thermal expansion coefficient α are given by [52]:

$$C_V = 3nk\left[4D\left(\frac{\theta}{T}\right) - \frac{3\theta/T}{e^{\theta/T} - 1}\right], \tag{30}$$

$$\alpha = \frac{\gamma C_V}{B_T V}. \tag{31}$$

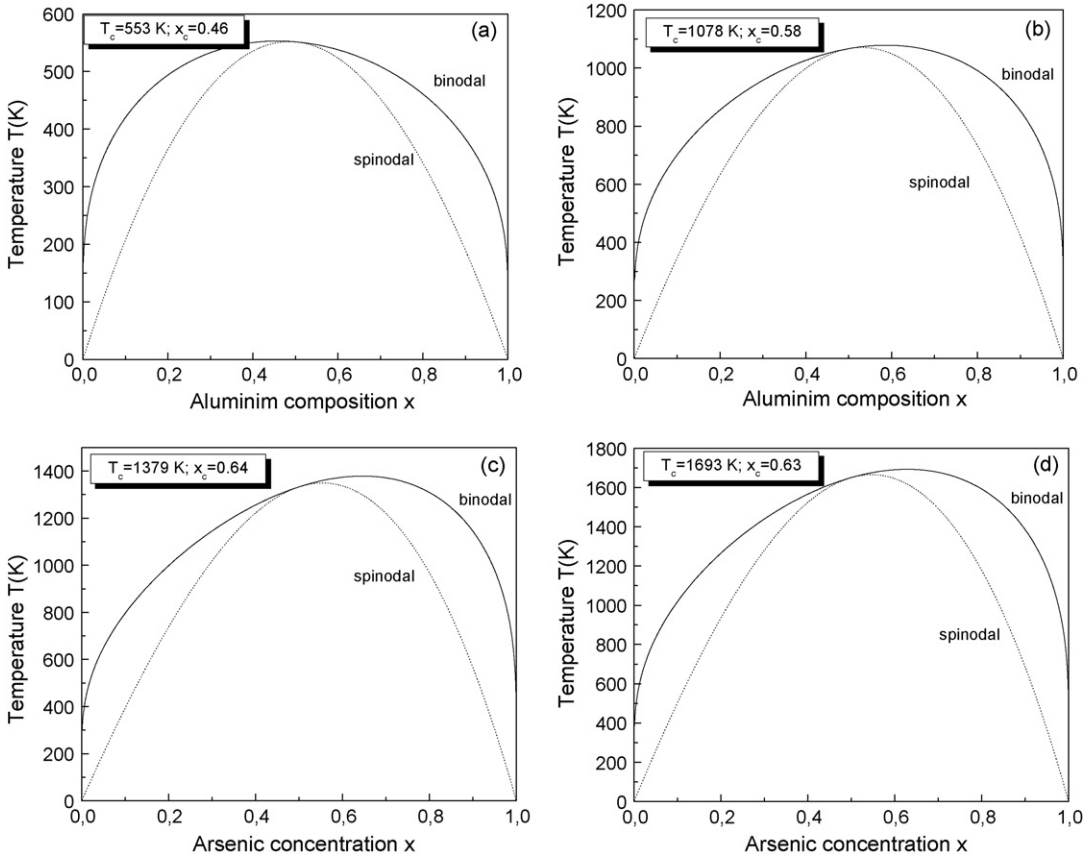

Fig. 7. Phase diagram as function of concentration for (a) $Al_xGa_{1-x}As$, (b) $Al_xGa_{1-x}Sb$, (c) $GaAs_xSb_{1-x}$ and (d) $AlAs_xSb_{1-x}$ ternary alloys. Solid curve: binodal, dotted curve: spinodal.

where is the Grüneisen parameter which is defined as

$$\gamma = -\frac{d\ln\theta(V)}{d\ln V}. \tag{32}$$

Through the quasi-harmonic Debye model, one could calculate the thermodynamic quantities of any temperatures and pressures of compounds from the calculated E–V data at $T = 0$ and $P = 0$.

The calculated Debye temperature θ at 300 K are depicted in Fig. 8. Accordingly, the increase of concentration x leads to the Debye temperature increase as well as the compressibility decrease (see Fig. 1). This result is in accordance with the fact that Debye temperature is proportional to the bulk modulus and that a hard material exhibits a high Debye temperature.

The vibrational properties which are related to the thermal effects are the heat capacity C_V and the thermal expansion

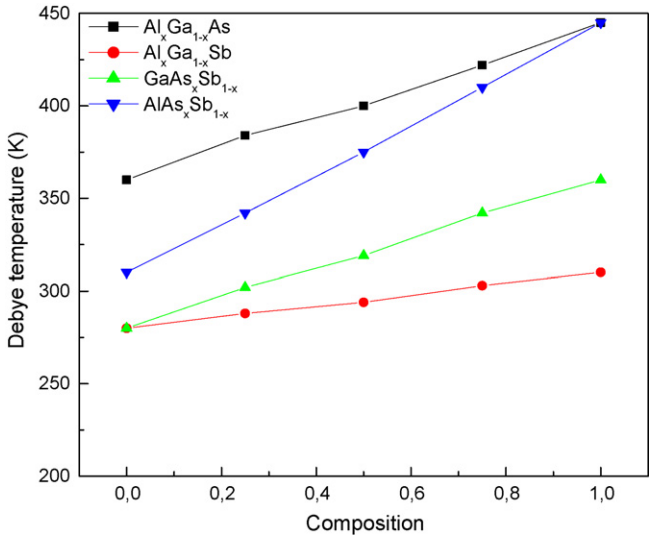

Fig. 8. The Debye temperature θ as function of concentration for the alloys of interest at room temperature.

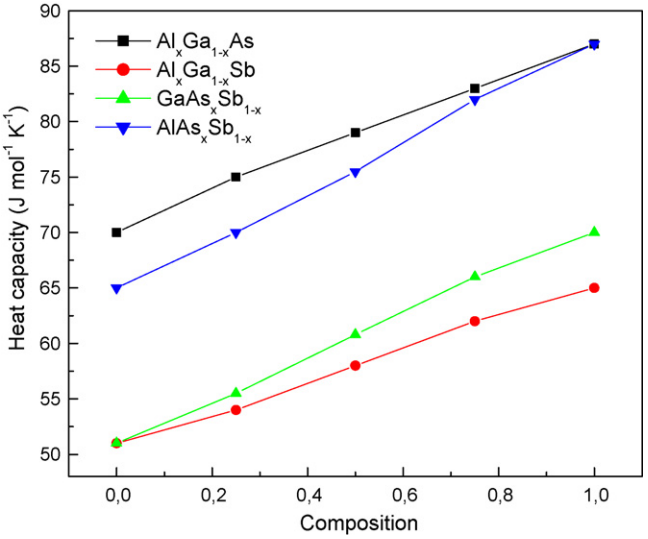

Fig. 9. The heat capacity C_V as function of concentration for the alloys of interest at room temperature.

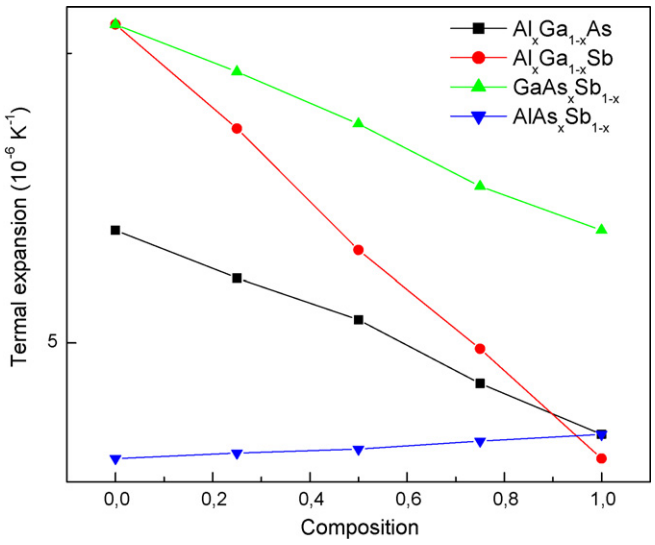

Fig. 10. The thermal expansion coefficient α as function of concentration for the alloys of interest at room temperature.

coefficient α. Our results concerning the heat capacity C_V at room temperature show a no linear behavior in Fig. 9. The x-dependent thermal expansion coefficient α at room temperature with a smooth variation was displayed in Fig. 10.

4. Conclusions

We have investigated the structural electronic, optical and thermodynamic properties of the $Al_xGa_{1-x}As$, $Al_xGa_{1-x}Sb$, $GaAs_xSb_{1-x}$ and $AlAs_xSb_{1-x}$ ternary alloys as a function of the composition x by using the FP-LAPW+lo method within DFT. A non-linear behavior of the lattice constant, bulk modulus and band gap dependence on x has been observed. Our results regarding the gap bowing of the ternary alloys are found to be in reasonable agreement with the experimental data. The investigation of the origin of the band gap bowing shows that this one is mainly dominated by the charge-transfer effect, while the volume deformation and the structural relaxation contribute at smaller magnitude. The critical point structure of the frequency, dependent complex dielectric function was investigated and analyzed to identify the optical transitions. The enthalpy of mixing ΔH_m is calculated in the whole composition range. The calculated ΔH_m is expressed within the regular-solution model using the x-dependent interaction parameter Ω. The calculated phase diagram indicates a significant phase miscibility gap. These results indicate that the four ternary alloys are unstable over a wide range of intermediate compositions at normal growth temperatures. Finally, the quasi-harmonic Debye model is successfully applied to determine the thermal properties at room temperature.

Acknowledgments

One of the authors (F.H.H.) would like to thank the Doctoral School of Sciences and Technology in the Lebanese university (EDST), Abdus Salam International Centre for Theoretical Physics (ICTP) and Metz University for their financial support during the realization of this work.

References

[1] U.K. Mishra, J. Singh, Semiconductor Device Physics and Design, Springer, Dordrecht, 2008.
[2] M. Othman, E. Kasap, N. Korozlu, J. Alloys Compd. (2009), doi:10.1016/j.jallcom.2009.12.109.
[3] K. Iga, S. Kinoshita, Process Technology for Semiconductor Lasers, Springer-Verlag, Berlin, 1996.
[4] M. Quillec, Materials for Optoelectronics, Kluwer Academic Publ, Boston, 1996.
[5] G. Guisbiers, M. Wautelet, L. Buchaillot, Phys. Rev. B 79 (2009) 155426.
[6] M. Levinshtein, S. Rumyantsev, M. Shur, Handbook Series on Semiconductor Parameters, Vol. 2, Ternary, and Quaternary III–V Compounds, World Scientific, 1999.
[7] N Bouarissa, Mater. Chem. Phys. 72 (2001) 387.
[8] I. Vurgaftman, J.R. Meyer, L.R. Ram-Mohan, J. Appl. Phys. 89 (2001) 5815.
[9] S. Adachi, J. Appl. Phys. 58 (1985) R1.
[10] H. Toyota, T. Sasaki, Y. Jinbo, N. Uchitomi, J. Cryst. Growth 310 (2008) 78.
[11] H. Yamaguchi, S. Miyashita, Y. Hirayama, Appl. Surf. Sci. 237 (2004) 649.
[12] A. Furukawa, M. Mizuta, Electron. Lett. 24 (1988) 1378.
[13] H. Xie, W.I. Wang, Appl. Phys. Lett. 63 (1993) 776.
[14] K.D. Moiseev, V.V. Romanov, T.I. Voronina, T.S. Lagunova, M.P. Mikhailova, Y.P. Yakovlev, J. Cryst. Growth 310 (2008) 4846.
[15] N. Bouarissa, Mater. Chem. Phys. 100 (2006) 41.
[16] J. Shin, T.C. Hsu, Y. Hsu, G.B. Stringfellow, J. Cryst. Growth 179 (1997) 1.
[17] M. Linnik, A. Christou, Physica B 318 (2002) 140.
[18] M.P.C.M. Krijn, Semicond. Sci. Technol. 6 (1991) 27.
[19] Y. Kawamura, H. Kurisu, K. Yoshimatsu, A. Kamada, Y. Naito, N. Inoue, Jpn. J. Appl. Phys. 36 (1997) 757.
[20] O. Ostinelli, G. Almuneau, W. Bächtold, Semicond. Sci. Technol. 21 (2006) 681.
[21] A. Zunger, S.-H. Wei, L.G. Ferreira, J.E. Bernard, Phys. Rev. Lett. 65 (1990) 353.
[22] D.D. Koelling, B.N. Harmon, J. Phys. C: Solid State Phys. 10 (1977) 3107.
[23] G.K.H. Madsen, P. Blaha, K. Schwarz, E. Sjöstedt, L. Nordström, Phys. Rev. B 64 (2001) 195134.
[24] K. Schwarz, P. Blaha, G.K.H. Madsen, Comput. Phys. Commun. 147 (2002) 71.
[25] P. Hohenberg, W. Kohn, Phys. Rev. 136 (1964) 864;
W. Kohn, L.J. Sham, Phys. Rev. A 140 (1965) 1133.
[26] P. Blaha, K. Schwarz, G.K.H. Madsen, D. Kvasnicka, J. luitz, WIEN2K, "an Augmented Plane Wave + Local orbitals program for calculating crystal properties" Karlheinz Schwarz, Techn. Universitat, Wien, Austria, 2008.
[27] Z. Wu, R.E. Cohen, Phys. Rev. B 73 (2006) 235116.
[28] J.P. Perdew, K. Burke, M. Ernzerhof, Phys. Rev. Lett. 77 (1996) 3865.
[29] E. Engel, S.H. Vosko, Phys. Rev. B 47 (1993) 13164.
[30] F.D. Murnaghan, Proc. Natl. Acad. Sci. U.S.A. 30 (1944) 244.
[31] K. Strössner, S. Ves, C.K. Kim, M. Cardona, Phys. Rev. B 33 (1986) 4044.
[32] F. El Haj Hassan, B. Amrani, J. Phys.: Condens. Matter 19 (2007) 386234.
[33] F. El Haj Hassan, H. Akbarzadeh, Comput. Mater. Sci. 35 (2006) 423.
[34] P. Dufek, P. Blaha, K. Schwarz, Phys. Rev. B 50 (1994) 7279.
[35] F. El Haj Hassan, S.J. Hashemifar, H. Akbarzadeh, Phys. Rev. B 73 (2006) 195202; F. El Haj Hassan, H. Akbarzadeh, S.J. Hashemifar, J. Phys.: Condens. Matter 16 (2004) 3329.
[36] L. Vegard, Z. Phys. 5 (1921) 17.
[37] B. Jobst, D. Hommel, U. Lunz, T. Gerhard, G. Landwehr, Appl. Phys. Lett. 69 (1996) 97.
[38] J.P. Dismuckes, L. Ekstrom, R.J. Poff, J. Phys. Chem. 68 (1964) 3021.
[39] F. El Haj Hassan, H. Akdarzadeh, Mater. Sci. Eng. B 121 (2005) 170.
[40] A. Zaoui, M. Ferhat, B. Khelifa, J.P. Dufour, H. Aourag, Phys. Stat. Sol. (b) 185 (1994) 163.
[41] F. El Haj Hassan, H. Akbarzadeh, M. Zoaeter, J. Phys.: Condens. Matter 16 (2004) 293.
[42] J.C. Phillips, Rev. Mod. Phys. 42 (1970) 317.
[43] V. Fiorentini, A. Baldereschi, Phys. Rev. B 51 (1995) 17196.
[44] O. Madelung, Semiconductors Basic Data, Springer, Berlin, 1996.
[45] J.E. Bernard, A. Zunger, Phys. Rev. B 34 (1986) 5992.
[46] W. Sargent, Table of Periodic Properties of the Elements, Sargent-Welch Scientific, Skokie, IL, 1980.
[47] C. Amrosch-Draxl, J.O. Sofo, Comput. Phys. Commun. 175 (2006) 1.
[48] R.A. Swalin, Thermodynamics of Solids, John Wiley & Sons, New York, 1961.
[49] M.A. Blanco, E. Francisco, V. Luaña, Comput. Phys. Commun. 158 (2004) 57.
[50] E. Francisco, J.M. Recio, M.A. Blanco, A. Martín Pendás, J. Phys. Chem. 102 (1998) 1595.
[51] E. Francisco, M.A. Blanco, G. Sanjurjo, Phys. Rev. B 63 (2001) 094107.
[52] R. Hill, Proc. Phys. Soc. Lond. A 65 (1952) 349.